Hydrol. Earth Syst. Sci., 24, 2105–2120, 2020
https://doi.org/10.5194/hess-24-2105-2020


Hydrology and Earth System Sciences
Open Access
EGU

# Age and origin of leaf wax *n*-alkanes in fluvial sediment–paleosol sequences and implications for paleoenvironmental reconstructions

**Marcel Bliedtner[1,2], Hans von Suchodoletz[3,4], Imke Schäfer[2], Caroline Welte[5], Gary Salazar[6], Sönke Szidat[6], Mischa Haas[7], Nathalie Dubois[8], and Roland Zech[1]**

[1]Institute of Geography, Friedrich Schiller University of Jena, Löbdergraben 32, 07743 Jena, Germany
[2]Institute of Geography and Oeschger Centre for Climate Change Research, University of Bern, 3012 Bern, Switzerland
[3]Institute of Geography, University of Technology Dresden, 01069 Dresden, Germany
[4]Institute of Geography, University of Leipzig, 04103 Leipzig, Germany
[5]Laboratory of Ion Beam Physics, ETH Zurich, 8093 Zurich, Switzerland
[6]Department of Chemistry and Biochemistry and Oeschger Centre for Climate Change Research, University of Bern, 3012 Bern, Switzerland
[7]Department of Surface Waters Research and Management, Eawag, 8600 Dübendorf, Switzerland
[8]Department of Earth Sciences, ETH Zürich, 8006 Zurich, Switzerland

**Correspondence:** Marcel Bliedtner (marcel.bliedtner@uni-jena.de)

Received: 22 May 2019 – Discussion started: 17 June 2019
Revised: 13 March 2020 – Accepted: 29 March 2020 – Published: 28 April 2020

**Abstract.** Leaf wax *n*-alkanes are increasingly used for quantitative paleoenvironmental reconstructions. However, this is complicated in sediment archives with associated hydrological catchments since the stored *n*-alkanes can have different ages and origins. $^{14}$C dating of the *n*-alkanes yields independent age information for these proxies, allowing their correct paleoenvironmental interpretation. This also holds true for fluvial sediment–paleosol sequences (FSPSs) that integrate two different *n*-alkane signals: (i) a catchment signal in fluvial sediments and (ii) an on-site signal from local biomass that increasingly dominates (paleo)soils with time. Therefore, the age and origin of *n*-alkanes in FSPSs are complex: in fluvial sediment layers they can be pre-aged and reworked when originating from eroded catchment soils or from organic-rich sediment rocks in the catchment. In (paleo)soils, besides an inherited contribution from the catchment, they were formed on-site by local biomass during pedogenesis. Depending on the different relative contributions from these sources, the *n*-alkane signal from an FSPS shows variable age offsets between its formation and final deposition.

During this study, we applied compound-class $^{14}$C dating to *n*-alkanes from an FSPS along the upper Alazani in eastern Georgia. Our results show that preheating the *n*-alkanes with 120 °C for 8 h before $^{14}$C dating effectively removed the shorter chains ($< C_{25}$) that partly originate from *n*-alkanes from Jurassic black clay shales in the upper catchment. The remaining petrogenic contributions on the longer chains ($\geq C_{25}$) were corrected for by using a constant correction factor that was based on the *n*-alkane concentrations in a black clay shale sample from the upper catchment. Due to different degrees of pre-aging and reworking, the corrected leaf wax *n*-alkane ages still indicate relatively large age offsets between *n*-alkane formation and deposition: while intensively developed (paleo)soils showed no age offsets due to a dominance of leaf wax *n*-alkanes produced on-site, less intensively developed paleosols showed much larger age offsets due to larger proportions of inherited leaf wax *n*-alkanes from the fluvial parent material. Accordingly, age offsets in nonpedogenic fluvial sediments were largest and strongly increased after ∼ 4 ka cal BP. The leaf wax *n*-alkane homolog distribution from intensively developed (paleo)soils indicates a local dominance of grasses and herbs throughout the Holocene, which was most likely caused by anthropogenic activity. The leaf wax *n*-alkanes from fluvial sediments show a dominance of deciduous trees and shrubs as well as grasses and herbs in different parts of the catchment between ∼ 8 and ∼ 5.6 ka cal BP. Since no older deciduous

tree- or shrub-derived $n$-alkanes were dated, this seems to confirm a delayed regional postglacial reforestation of parts of the catchment compared with western and central Europe.

## 1 Introduction

Long-chain $n$-alkanes ($\geq C_{25}$) that are biosynthesized as epicuticular leaf waxes by higher terrestrial plants are valuable biomarkers in paleoenvironmental research. They stay well preserved in soils and sediment archives because of their low water solubility, their chemical inertness and their persistence against degradation (Eglinton and Eglinton, 2008). The homolog distribution of leaf wax $n$-alkanes, as well as their stable hydrogen and carbon isotopic composition, is used as a novel proxy to quantitatively reconstruct past changes in vegetation and hydroclimatic conditions from various sediment archives, including lake sediments (Sauer et al., 2001; Schwark et al., 2002; Sachse et al., 2006; Wirth and Sessions, 2016), loess–paleosol sequences (Schäfer et al., 2018; Häggi et al., 2019), marine sediments (Schefuß et al., 2005) and fluvial sediment sequences (Bliedtner et al., 2018a). However, reconstructions from sediment archives with associated hydrological catchments can be complicated by the fact that sediments and leaf wax $n$-alkanes transit through the catchment over hundreds to several thousands of years, and thus the timing of their deposition does not necessarily reflect the timing of leaf wax $n$-alkane formation (Smittenberg et al., 2006; Feng et al., 2013; Douglas et al., 2014, 2018; Gierga et al., 2016). Resulting age offsets between leaf wax $n$-alkane formation and deposition will therefore limit any quantitative paleoenvironmental reconstruction.

In general, organic carbon (OC) and $n$-alkanes that are preserved in fluvial, lacustrine and marine sediment archives can originate from different sources (Hedges et al., 1986). They can (i) directly derive from recent to subrecent plant biomass, (ii) be pre-aged and reworked when derived from eroded catchment soils that were formed before their erosion and final deposition in the sediment archive (Blair and Aller, 2012) and (iii) originate from organic-rich sediment rocks. This highly aged petrogenic organic material has undergone alteration and has to be regarded as fossil; i.e. it is $^{14}$C dead (Galy et al., 2008; Hilton et al., 2010). Additionally, $n$-alkanes can originate from recent to subrecent aquatic production or from microbial production and postsedimentary microbial utilization (Ficken et al., 2000; Makou et al., 2018). These different sources of OC and $n$-alkanes explain the wide range of $^{14}$C ages that are reported in the literature for riverine-transported particulate organic matter, leaf wax $n$-alkanes and $n$-alkanoic acids (Galy and Eglinton, 2011; Marwick et al., 2015; Tao et al., 2015; Schefuß et al., 2016). Age offsets between leaf wax $n$-alkane formation and deposition on the order of hundreds to thousands of years were mostly reported from lake sediments so far and seem to increase throughout the Holocene due to anthropogenically induced soil erosion (Douglas et al., 2014; Gierga et al., 2016).

Possibilities to investigate the sources of OC and $n$-alkanes and to track their way through hydrological catchments have been made possible by the development of the Mini Carbon Dating System (MICADAS), which is an accelerator mass spectrometer (AMS) equipped with a hybrid ion source. When coupled to an elemental analyzer (EA), the MICADAS enables online $^{14}$C analyses of combustible samples with very small amounts of carbon (Wacker et al., 2010; Ruff et al., 2011, Welte et al., 2018). Thus, the EA–MICADAS allows $^{14}$C dating of specific OC compounds, such as specific leaf wax $n$-alkane compounds. However, because compound-specific $^{14}$C dating requires specialized equipment (preparative gas chromatography) and is very labor- and cost-intensive, compound-class $^{14}$C dating in which the whole $n$-alkane fraction is dated has been proposed as an elegant and cost-effective alternative, at least for loess–paleosol sequences (Haas et al., 2017; Zech et al., 2017).

Up to now, the age and origin of leaf wax $n$-alkanes have not been investigated in fluvial sediment–paleosol sequences (FSPSs), although such archives can be found ubiquitously in many regions of the world and have great potential for leaf wax $n$-alkane-based paleoenvironmental reconstructions (Bliedtner et al., 2018a). In such sequences, the fluvial sediments were deposited during phases of geomorphic activity with intensive flooding and contain $n$-alkanes that carry a mixed catchment signal. In contrast, the paleosols were formed during phases of geomorphic stability when no or much fewer fluvial sediments were deposited. Besides catchment-derived $n$-alkanes from previous fluvial sedimentation, they contain $n$-alkanes that derive from local biomass and thus carry an on-site signal (Bliedtner et al., 2018a). Therefore, $n$-alkanes in FSPSs have a complex origin and can either have formed on-site during soil formation, be pre-aged and reworked or originate from petrogenic sources when derived from the catchment. Additionally, microbial production and utilization can potentially contribute to both the $n$-alkanes produced on-site and the $n$-alkanes derived from the catchment. Depending on different relative contributions from these sources, the $n$-alkane signal recorded in FSPSs can be older than the timing of sedimentation since it integrates over different temporal and spatial scales, and the resulting age offsets can vary throughout the profile.

Here we investigated $^{14}$C ages of $n$-alkanes from an FSPS along the upper Alazani in eastern Georgia. Besides leaf-wax-derived $n$-alkanes, $^{14}$C-dead petrogenic $n$-alkanes from Jurassic black clay shales without a distinct odd-over-even predominance (OEP) from the upper Alazani subcatchment also contribute to all chain lengths of the $n$-alkane signal in the FSPS ($C_{21}$–$C_{35}$) (Bliedtner et al., 2018a). Since those petrogenic $n$-alkanes contribute with a strongly depleted $^{14}$C signal (i.e., they are $^{14}$C dead) to the leaf-wax-derived $n$-alkanes, they should lead to increased age offsets and will therefore complicate compound-class $^{14}$C dating of

the $n$-alkanes as a whole fraction. Therefore, to overcome this limitation we (i) removed the mostly petrogenic short-chain $n$-alkanes ($< C_{25}$) in our samples by a preheat treatment and (ii) subsequently applied a simple correction approach for the remaining petrogenic contributions that underlie the long-chain $n$-alkanes ($\geq C_{25}$) that mostly originate from Quaternary leaf waxes. We hypothesized that due to pre-aging effects, i.e., reworking of soil-derived leaf wax $n$-alkanes from the upper Alazani subcatchment, the remaining age offsets should be larger for the fluvial sediment layers compared with the well-developed paleosols that contain a high proportion of $n$-alkanes produced on-site. Doing so, we wanted to (i) evaluate the potential of $n$-alkane $^{14}$C dating in FSPSs after removing the petrogenic contribution, (ii) disentangle the different $n$-alkane sources and pathways before deposition and (iii) directly date the $n$-alkane proxies in our investigated FSPS for more robust paleoenvironmental interpretations.


**Figure 1.** Overview of the Caucasus region. The red rectangle marks the study area in the upper Alazani valley. Regional pollen records that are used for comparison in this study are marked with a white dot: 1 = Lake Paravani (Messager et al., 2013), 2 = Sagarejo sediment section (Gogichaishvili, 1984), 3 = Lake Van (Litt et al., 2009), 4 = Lake Urmia (Bottema, 1986).

## 2 Material and methods

### 2.1 Studied site

The investigated FSPS (42°02′17.7″ N, 45°21′18.7″ E; 450 m a.s.l.) is located in the upper Alazani valley in eastern Georgia. The Alazani river originates at an altitude of ∼ 2800 m a.s.l. from the southern slopes of the Greater Caucasus Mountains (Figs. 1 and 2a). The Alazani flows from north to south for the first ∼ 40 km and then, after its confluence with the smaller Ilto River, follows the NW–SE-oriented Alazani thrust top basin for ∼ 160 km (Fig. 2a). Here the Alazani is paralleled by the southern foothills of the Greater Caucasus in the northeast (Adamia et al., 2010) and the southwesterly advancing Kura fold-and-thrust belt (Kura FTB) in the southwest (Forte et al., 2010) (Figs. 1 and 2a). Finally, the ∼ 240 km long Alazani drains via the Kura into the Caspian Sea (Fig. 1). The investigated FSPS is located in the upper part of the Alazani thrust top basin, ca. 10 km downstream of the confluence of the Ilto and upper Alazani (Fig. 2a). Upstream of this site both rivers show a braided character and are thus characterized by coarse gravelly river beds. The site-related subcatchment in the upper Alazani and Ilto valleys is mountainous with a relatively small size of ∼ 1100 km$^2$. It shows quite steep slopes with an average slope angle of ∼ 20°, and especially in the uppermost part slopes up to 50° are found (Bliedtner et al., 2018a; Fig. 2a and b). The uppermost part of the upper Alazani subcatchment in the central southern Greater Caucasus is formed by folded and metamorphosed Jurassic flysch and molasse deposits that consist of altered organic-rich black clay shales, sand- and siltstone, and volcanic rock (Fig. 2c). Following downstream, the middle part of the upper Alazani subcatchment is dominated by Cretaceous sand-, silt- and limestone. The southern part of the subcatchment is dominated by the Kura FTB, which reaches altitudes of 2000 m and consists of folded and overthrusted Cretaceous sand-, silt- and limestone and Paleogene to Quaternary sandstone, siltstone and conglomerates (Gamkrelidze, 2003; Fig. 2c). Brownish loamy slope deposits are found in parts of the lower Ilto subcatchment that probably originate from Late Pleistocene eolian loess (Bliedtner et al., 2018a; Fig. 2c).

At the studied site, the recent mean annual temperature and precipitation are about 12.0 °C and 720 mm a$^{-1}$, respectively (http://de.climate-data.org/location/28480/, last access: 24 April 2020, station: Akhmeta). In the upper Alazani subcatchment, precipitation reaches up to 2000 mm a$^{-1}$ because most parts are located in the central southern Greater Caucasus (unpublished precipitation map from the Vakhushti Bagrationi Institute of Geography in Tbilisi). Precipitation mainly falls in spring and early summer during convective events (Lydolph, 1977), and thus the Alazani reaches its maximal discharge between April and June due to both snowmelt in the Greater Caucasus and the concomitant precipitation maximum; i.e., there is a pluvionival runoff regime (von Suchodoletz et al., 2018).

The recent vegetation of eastern Georgia belongs to the Irano-Turanian group (Connor et al., 2004; Sagheb-Talebi et al., 2014). The natural vegetation of the floodplains in the upper Alazani valley, where the studied site is located, consists of deciduous elm–oak–vine forests (Connor and Kvavadze, 2008). However, agricultural fields and grasslands cover most of the recently inactive elevated valley floor that is outcropped by the investigated FSPS today, whereas the lower-lying active modern floodplain hosts scattered patches of deciduous riparian forests. The mid-mountain belt further upstream is characterized by mixed beech and in small parts also by fir–spruce forests. Alpine to subalpine mead-

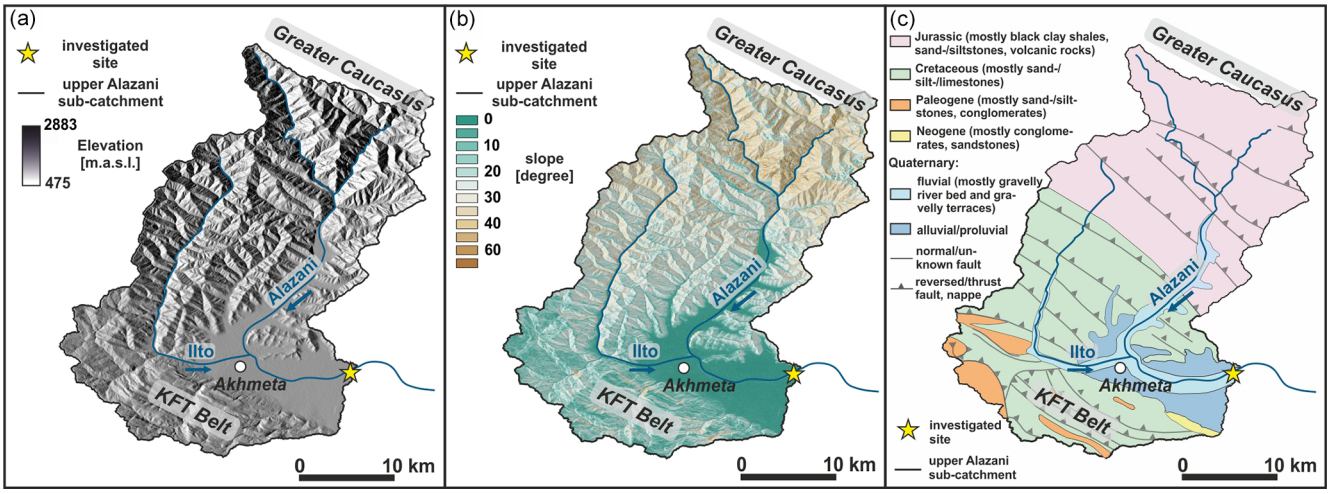


**Figure 2. (a)** Digital elevation model of the upper Alazani subcatchment (SRTM30-DEM). **(b)** Slope map of the upper Alazani subcatchment. **(c)** Geological map of the upper Alazani subcatchment (simplified after Gamkrelidze, 2003). KFT belt: Kura fold-and-thrust belt.

ows cover the highest parts of the catchment (Connor and Kvavadze, 2008). Today, ∼ 65 % of the upper Alazani subcatchment is covered by forests and ca. 35 % by grasslands and fields (Bliedtner et al., 2018a).

### 2.2 Stratigraphy of the investigated FSPS

The investigated FSPS is naturally exposed up to ∼ 7 m along the upper Alazani and consists mostly of fine-grained overbank sediments with intercalated paleosols. The sequence was previously investigated by von Suchodoletz et al. (2018), where a more detailed description can be found. Throughout the sequence, six blackish-grayish to reddish paleosols were developed in the fine-grained silty to clayey overbank sediments (Fig. 3). Three intensively developed paleosols are characterized by distinct upper but gradual lower limits (Ahb1, Ahb5, Ahb6), whereas three weakly developed paleosols (Ahb2, Ahb3, Ahb4) only showed gradual upper and lower limits. A well-developed recent soil (Ah) covers the surface of the sequence. The sediments of the FSPS were previously analyzed for carbonate content, total organic carbon (TOC), pH and mass-specific magnetic susceptibility ($\chi$) to differentiate paleosols formed on-site from partly similar-looking fluvial sediments. Based on a relative soil development index (SDI), the differences in these measured values from the uppermost sample of a paleo(soil) to the underlying parent material were averaged to calculate soil development intensities (von Suchodoletz et al., 2018). All paleosols are characterized by systematically decreasing carbonate content and pH values and increasing TOC content and $\chi$ values from bottom to top.

The chronology of the FSPS is based on nine charcoal pieces that were dated with $^{14}$C (Fig. 3). The $^{14}$C ages are in stratigraphic order except two samples that are older than stratigraphically lower samples. Therefore, they must overestimate their true burial age; i.e., they might have been reworked. Apart from these two samples, the charcoal chronology of the FSPS represents the timing of sediment deposition and soil development and serves as an independent age control for comparison with leaf wax *n*-alkane $^{14}$C ages (Fig. 3). The chronology ranges between 8.0–8.2 ka cal BP (95.4 %) in the upper part of Ahb6 and 1.6–1.8 ka cal BP (95.4 %) in the sediments below the recent soil Ah. The oldest $^{14}$C age of 8.0–8.2 ka cal BP (95.4 %) was obtained from a charcoal piece that was found together with archeological artifacts (potsherds, bones, obsidian tools) in the upper part of Ahb6. This documents anthropogenic activity at this site at least since the Neolithic period. Based on the $^{14}$C age of 1.6–1.8 ka cal BP (95.4 %) from the nonpedogenic fluvial sediments below the recent soil Ah, the time to form the Ah was estimated to be ca. 1.6 kyr. This age was used as a reference to calculate the approximate soil forming durations for the paleosols based on the soil development index (SDI). For more detailed information how the SDI was derived, the reader is referred to von Suchodoletz et al. (2018).

### 2.3 Analytical procedure

#### 2.3.1 *n*-Alkane extraction, separation and quantification

A total of 24 samples from the FSPS along the upper Alazani were previously analyzed over the whole profile for their *n*-alkane homolog distributions (Bliedtner et al., 2018a). Five of these samples were used for this study as a pretest (step 1; see below). These samples were extracted with accelerated solvent extraction as described by Bliedtner et al. (2018a). Based on this pretest, 11 samples from the FSPS, including four from the pretest, were extracted again using an ultrasonic treatment according to Bliedtner et al. (2018b) (step 2;

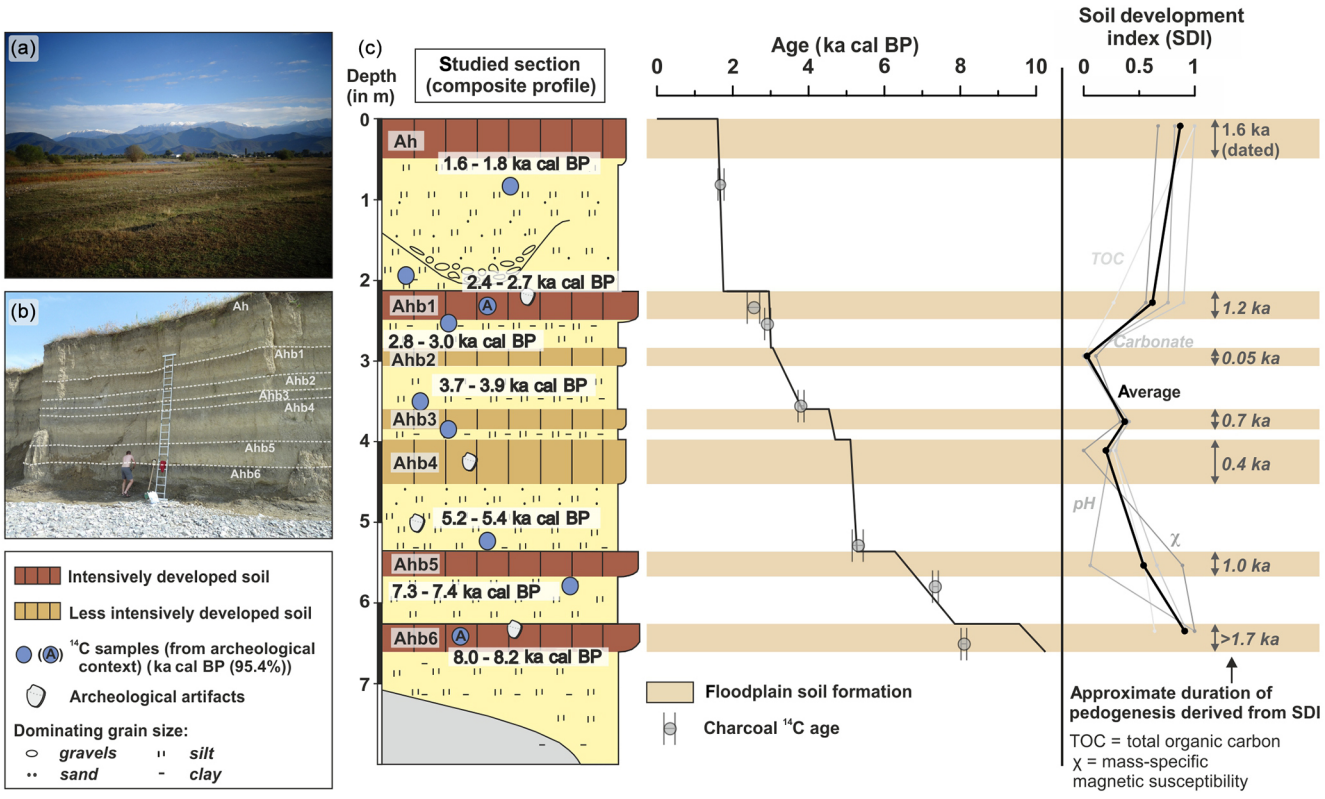


**Figure 3.** **(a)** Photo of the active modern floodplain next to the investigated FSPS in the front and the mountainous upper Alazani catchment in the southern Greater Caucasus in the back. **(b)** Photo of the investigated FSPS with highlighted (paleo)soils. **(c)** Schematic stratigraphy of the investigated FSPS (left) with the age–depth model based on $^{14}$C datings of charcoal pieces (center) and approximate durations of soil formation based on a soil development index (SDI) (right; von Suchodoletz et al., 2018). The two charcoal samples that overestimated their burial ages were excluded from the age–depth model. Charcoal $^{14}$C ages are given as calibrated age ranges in ka cal BP (95.4 %) with the calibrated median age.

see below). To guarantee stratigraphical representativeness, six of these re-extracted samples were chosen from (paleo)soils and five from fluvial sediment layers.

All samples for $^{14}$C dating were extracted from air-dried and sieved (< 2 mm) sample material. The total lipid extracts of all samples were separated over aminopropyl pipette columns into (i) the apolar fraction including the *n*-alkanes, (ii) the more polar fraction and (iii) the acid fraction. The *n*-alkanes were eluted with ∼ 4 mL hexane and subsequently purified over coupled silver-nitrate ($AgNO_3$–)–zeolite pipette columns. The subsequent dating approach encompassed two steps:

1. First, the *n*-alkane fractions of five samples (Ala 25 I, 225 I, 290 I, 425 I, 505 I) were tested for compound-class $^{14}$C dating (i.e., $^{14}$C dating of the whole *n*-alkane fraction) during the pretest (see Table 1; samples with BE no.): whereas the *n*-alkane fractions of four samples were not heated prior to $^{14}$C measurement, the *n*-alkane fraction of sample Ala 25 I was preheated with 120 °C for 8 h. The preheating of the *n*-alkane fraction was carried out in a 1.5 mL GC vial, and the GC vial was placed into an oven at 120 °C for 8 h. The heated *n*-alkane fraction yielded a much younger $^{14}$C age compared with the other samples since the short-chain *n*-alkanes containing a significant petrogenic *n*-alkane contribution ($< C_{25}$) were effectively removed (see Table 1 and Sect. 3).

2. Based on the results of the pretest, the *n*-alkane fractions of the 11 re-extracted samples were also preheated with 120 °C for 8 h and subsequently $^{14}$C dated (see Table 1; samples with ETH no.). For direct comparison of the effectiveness of the preheating approach, *n*-alkane fractions of four re-extracted samples were taken from the same depths of the investigated FSPS as those from the pretest that were not previously heated.

The *n*-alkanes were identified and quantified using a gas chromatograph (Agilent 7890 with an Agilent HP5MS column) equipped with a flame ionization detector (GC–FID). For identification and quantification, external *n*-alkane standards ($C_{21}$–$C_{40}$) were run with each sequence.

**Table 1.** $n$-Alkane $^{14}$C ages from the investigated FSPS along the upper Alazani including treatment, carbon mass, fraction modern values ($F^{14}$C), uncalibrated $^{14}$C ages and calibrated $^{14}$C ages as calibrated age ranges in cal BP (95.4 %) with the calibrated median age. The $n$-alkane samples from the pretest are marked with I, whereas the corresponding reanalyzed $n$-alkane samples are marked with II for direct comparison. Rows written in bold indicate $n$-alkane samples from (paleo)soils.

| Lab. code | Sample label | Pre-treatment | Depth (cm) | Mass (µg) | $F^{14}$C | Uncalibrated ages | Calibrated age ranges (cal BP) | Calibrated median ages (cal BP) |
|---|---|---|---|---|---|---|---|---|
| **BE-4788.1.1** | **Ala 25 I** | **Heated** | **25** | **30** | **0.7865 ± 0.0110** | **1929 ± 112** | **1573–2150 (95.4 %)** | **1877** |
| ETH-81313.1.1 | Ala 100 | Heated | 100 | 49 | 0.4490 ± 0.0175 | 6432 ± 311 | 6660–7934 (95.4 %) | 7304 |
| **BE-4792.1.1** | **Ala 225 I** | **Not heated** | **225** | **55** | **0.5199 ± 0.0066** | **5255 ± 101** | **5756–6282 (95.4 %)** | **6046** |
| **ETH-81312.1.1** | **Ala 225 II** | **Heated** | **225** | **60** | **0.6583 ± 0.0159** | **3359 ± 193** | **3083–4150 (95.4 %)** | **3623** |
| ETH-81311.1.1 | Ala 280 | Heated | 280 | 54 | 0.3544 ± 0.0174 | 8334 ± 390 | 8390–10 264 (95.4 %) | 9310 |
| **BE-4793.1.1** | **Ala 290 I** | **Not heated** | **290** | **47** | **0.4148 ± 0.0082** | **7069 ± 158** | **7595–8191 (95.4 %)** | **7895** |
| **ETH-81310.1.1** | **Ala 290 II** | **Heated** | **290** | **55** | **0.4974 ± 0.0164** | **5610 ± 263** | **5769–7156 (95.3 %)** | **6427** |
| ETH-81309.1.1 | Ala 315 | Heated | 315 | 41 | 0.3598 ± 0.0205 | 8212 ± 452 | 8170–10 371 (95.4 %) | 9181 |
| ETH-81308.1.1 | Ala 390 | Heated | 390 | 47 | 0.4050 ± 0.0186 | 7261 ± 366 | 7468–8987 (95.4 %) | 8120 |
| **BE-4795.1.1** | **Ala 425 I** | **Not heated** | **425** | **47** | **0.2564 ± 0.0065** | **10 935 ± 203** | **12 430–13 255 (95.4 %)** | **12 850** |
| **ETH-81307.1.1** | **Ala 425 II** | **Heated** | **425** | **37** | **0.4553 ± 0.0208** | **6319 ± 363** | **6415–7927 (95.4 %)** | **7183** |
| BE-4796.1.1 | Ala 505 I | Not heated | 505 | 37 | 0.1866 ± 0.0048 | 13 488 ± 206 | 15 685–16 930 (95.4 %) | 16 257 |
| ETH-81306.1.1 | Ala 505 II | Heated | 505 | 27 | 0.4351 ± 0.0271 | 6685 ± 494 | 6494–8584 (95.4 %) | 7565 |
| **ETH-81305.1.1** | **Ala 545** | **Heated** | **545** | **31** | **0.4253 ± 0.0243** | **6867 ± 454** | **6749–8715 (95.4 %)** | **7753** |
| **ETH-81303.1.1** | **Ala 625** | **Heated** | **625** | **36** | **0.3782 ± 0.0220** | **7811 ± 463** | **7743–9887 (95.4 %)** | **8748** |

### 2.3.2 $^{14}$C measurements

For compound-class $^{14}$C dating, purified non-heated and preheated $n$-alkane fractions were transferred with dichloromethane into tin capsules (3.5 mm × 5.5 mm × 0.1 mm). $^{14}$C dating was performed on the Mini Carbon Dating System (MICADAS) AMS coupled online to an elemental analyzer (Wacker et al., 2010; Ruff et al., 2011). Results are reported as fraction modern ($F^{14}$C), which is the activity ratio of a sample related to the modern reference material oxalic acid II after subtracting the background signal.

The $n$-alkanes of the pretest (step 1) were analyzed at the LARA AMS Laboratory of the University of Bern, Switzerland (Szidat, 2014; BE no.). $F^{14}$C results from the LARA AMS were corrected for cross (carryover from sample to sample) and constant contamination (carbon mass and $F^{14}$C of the tin caps) according to the contamination drift model of Salazar et al. (2015). For constant contamination, 10 combined tin capsules were measured, which yielded 0.43 µg C for a single cap with $F^{14}$C values of 0.759.

The re-extracted and preheated $n$-alkane fractions (step 2) were analyzed at the LIP AMS of the ETH Zurich, Switzerland (ETH no.). $F^{14}$C results were corrected for constant contamination according to Welte et al. (2018) with a fossil $n$-alkane standard ($C_{28}$ with $F^{14}C = 0$) and a modern $n$-alkane standard ($C_{32}$ with $F^{14}C = 1.073$). Constant-contamination correction yielded 4.3 µg C for a single cap, with $F^{14}$C values of 0.895.

All $^{14}$C ages were calibrated to cal yr BP (95.4 % range) with the IntCal13 calibration curve (Reimer et al., 2013) using OxCal (Ramsey, 2009). Calibrated $^{14}$C ages were reported as age ranges following the conventions of Millard (2014). Additionally, we gave the $^{14}$C median age to the respective $^{14}$C age ranges. We also need to emphasize that compound-class dating of the $n$-alkanes in our fluvial sediment sequence might integrate over different spatial and temporal scales, which might complicate absolute age dating. However, since our main aim was to test the chronostratigraphic integrity of our $n$-alkanes in the fluvial sequence by comparing them with an independent charcoal-based $^{14}$C chronology that gives the timing of sedimentation, calibrated $^{14}$C ages seem to be best suited for comparison between our different types of $^{14}$C ages.

## 3 Results and discussion

Our study investigates $^{14}$C ages of $n$-alkanes from an FSPS along the upper Alazani and aims to (i) evaluate the potential of $n$-alkane $^{14}$C dating in FSPSs, (ii) disentangle the different $n$-alkane sources and pathways before deposition and (iii) date the $n$-alkane proxies in the FSPS for more robust paleoenvironmental reconstructions. Therefore, in the following we will present a preheat treatment and correction approach to remove the petrogenic $n$-alkane contribution from the leaf-wax-derived $n$-alkanes, discuss different pathways of leaf wax $n$-alkanes before their deposition and finally derive paleoenvironmental implications.

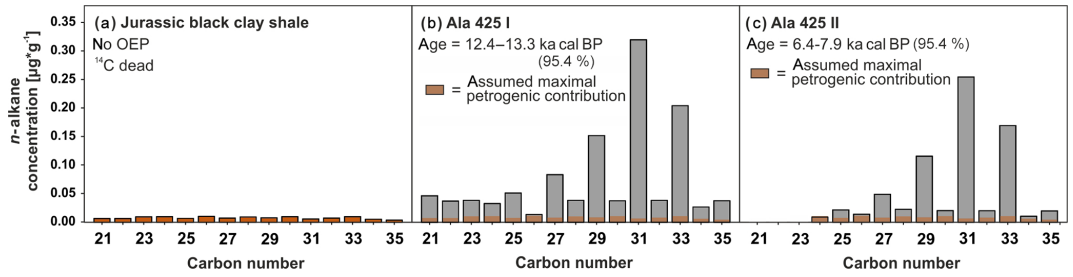


**Figure 4.** *n*-Alkane chain-length distributions in µg g$^{-1}$ sediment for **(a)** a Jurassic black clay shale sample from the upper Alazani subcatchment, **(b)** FSPS sediment sample Ala 425 I without heating and **(c)** re-extracted FSPS sediment sample Ala 425 II after heating with 120 °C for 8 h. *n*-Alkane $^{14}$C ages for samples Ala 425 I and II are given as age ranges in ka cal BP (95.4 %).

### 3.1 Heating experiments

Figure 4a shows the homolog distribution of petrogenic *n*-alkanes derived from a Jurassic black clay shale sample from the upper Alazani subcatchment (Fig. 2c). These are present with similar amounts at all chain lengths ($C_{21}$–$C_{35}$) and do not show a distinct odd-over-even predominance (OEP). These $^{14}$C-dead *n*-alkanes also contribute to the sedimentary leaf wax *n*-alkanes in our FSPS and are exemplarily shown as the assumed maximal petrogenic contribution for the *n*-alkane homolog distribution of nonheated sample Ala 425 I in Fig. 4b. During the pretest, this sample gave a $^{14}$C age of 12.4–13.3 ka cal BP (95.4 %), which is much older than the timing of sedimentation obtained from the charcoal $^{14}$C ages (∼ 5 to 4 ka cal BP). To at least partly reduce the contamination with petrogenic *n*-alkanes, we re-extracted this sample and applied the heat treatment of 120 °C for 8 h before $^{14}$C measurement. The *n*-alkane homolog distribution of the re-extracted and heated sample Ala 425 II (Fig. 4c) demonstrates that the short-chain *n*-alkanes and thus a significant amount of the petrogenic *n*-alkanes were effectively removed by this procedure. Consequently, the resulting $^{14}$C age of 6.4–7.9 ka cal BP (95.4 %) was much younger than the age obtained without preheating (Figs. 4c and 5).

The $^{14}$C ages of the other samples that were also measured both before and after the removal of the short-chain *n*-alkanes by heating were as follows: 5.8–6.3 ka cal BP (95.4 %) (Ala 225 I) and 3.1–4.2 ka cal BP (95.4 %) (Ala 225 II) for sample Ala 225, 7.6–8.2 ka cal BP (95.4 %) (Ala 290 I) and 5.8–7.2 ka cal BP (95.4 %) (Ala 290 II) for sample Ala 290, and 15.7–16.8 ka cal BP (95.4 %) (Ala 505 I) and 6.5–8.6 ka cal BP (95.4 %) (Ala 505 II) for sample Ala 505, respectively (Table 1; Fig. 5).

The results of our heating experiments show that here a simple heat treatment effectively removes the short-chain *n*-alkanes that contain a significant petrogenic component. However, we have to mention that no extensive heating experiments were carried out for the removal of short-chain *n*-alkanes prior to this study and that we only tested at three different temperatures (100, 110 and 120 °C) for 8 h.

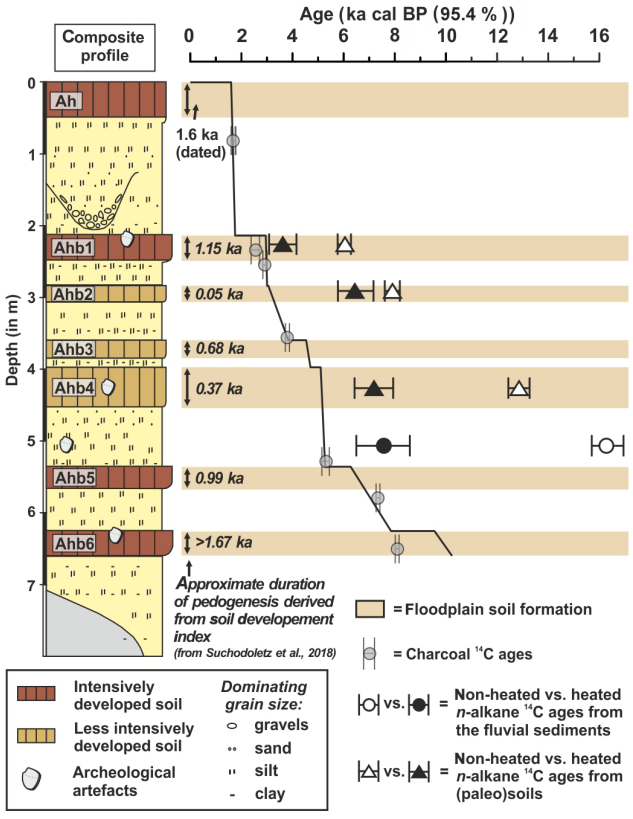


**Figure 5.** Comparison of nonheated *n*-alkane $^{14}$C ages from the pretest and heated *n*-alkane $^{14}$C ages that were re-extracted from the same samples of the investigated FSPS and heated with 120 °C for 8 h. For comparison, the independent age model based on $^{14}$C-dated charcoal pieces and the soil development index (SDI) is also shown (von Suchodoletz et al., 2018). $^{14}$C ages are given as calibrated age ranges in ka cal BP (95.4 %) with the calibrated median age.

We found that most of the short-chain *n*-alkanes could best be removed at 120 °C for 8 h, although a slight proportion of the longer chains was also removed. We also have to mention that possible fractionation during heating could potentially lead to an enrichment of the heavier $^{14}$C isotope, but such a fractionation effect should be negligible because the

$F^{14}C$ results were generally corrected for mass-dependent fractionation by the $^{13}C$ isotopes. Therefore, the applied heat treatment is an effective pretreatment to derive a more homogeneous leaf wax $n$-alkane signal for compound-class $^{14}C$ dating in general and especially in environmental settings where petrogenic OC and $n$-alkanes occur. Because of the partly removed petrogenic contribution, the $^{14}C$ age of a heated sample is generally closer to its leaf-wax-derived $n$-alkane $^{14}C$ age. However, since petrogenic $n$-alkanes are also present at the longer chains $\geq C_{25}$ that mostly originate from leaf waxes and serve as paleoenvironmental proxies (see Fig. 4), this pretreatment cannot completely remove the petrogenic contribution.

Furthermore, we have to mention that beside $n$-alkane contributions from petrogenic sources, short-chain $n$-alkane contributions from aquatic and microbial sources were also reported from lake sediments (Ficken et al., 2000; Makou et al., 2018), and microbial utilization was reported to alter the leaf wax signal of the longer chains (Li et al., 2018). While we cannot completely rule out possible aquatic and microbial contributions to our leaf-wax-derived $n$-alkanes, we suggest that such contributions are negligible in our fluvial sediment sequence. This is because $n$-alkanes from aquatic and microbial production would show a clear OEP on the shorter chains with younger $^{14}C$ ages, whereas our short-chain $n$-alkanes show no OEP and the $^{14}C$ ages become significantly younger after the removal of the shorter chains by heating.

### 3.2 $n$-Alkane $^{14}C$ ages from the FSPS along the upper Alazani

In the following, we will only focus on the 11 $n$-alkane samples from the investigated FSPS that were preheated with 120 °C for 8 h. $n$-Alkanes were present in all these samples after heating, with values ranging between 27 and 60 µg carbon per $n$-alkane fraction, which was enough carbon for robust $^{14}C$ measurements. Their $F^{14}C$ values range from $0.7865 \pm 0.0110$ to $0.3544 \pm 0.0174$, what corresponds to calibrated calendar ages from 1.6–2. ka cal BP (95.4 %) to 8.4–10.7 ka cal BP (95.4 %) (Table 1).

Calibrated calendar ages for the $n$-alkanes from (paleo)soils and fluvial sediment layers are shown in Fig. 6. Compared to the independent charcoal-based $^{14}C$ chronology of the sequence (von Suchodoletz et al., 2018), the $n$-alkane $^{14}C$ ages show variable age offsets over the FSPS; i.e., they are generally older. The $n$-alkane $^{14}C$ ages of intensively developed paleosols and the recent soil show generally lower age offsets (between 0 and 1.3 ka) than those from less intensively developed paleosols (up to 3.3 ka) (Fig. 6). The age offsets of the $n$-alkanes from fluvial sediment layers are generally older than those from all (paleo)soils and increase in the upper part of the FSPS (Fig. 6). Age offsets in the lower part range between $\sim$ 2.3 and 3.5 ka and increase to up to $\sim$ 6 ka in the upper part.

### 3.3 Estimation and correction for petrogenic $n$-alkanes

Our preheating of the $n$-alkane fractions with 120 °C for 8 h effectively removed the short-chained petrogenic $n$-alkanes ($< C_{25}$) derived from Jurassic black clay shales in the upper Alazani subcatchment. However, such petrogenic $n$-alkanes are also present at the longer chains ($C_{25}$–$C_{35}$), where they underlie the leaf-wax-derived $n$-alkanes and do not show a distinct OEP (see Fig. 4c). Our preheating can therefore not fully remove all petrogenic $n$-alkanes. To correct for this underlying petrogenic contribution, we propose a simple correction procedure that uses a constant correction factor: a measured Jurassic black clay shale sample from the upper Alazani subcatchment yielded an average concentration of $0.007\,\mu g\,g^{-1}$ per single $n$-alkane compound (see Fig. 4a). Assuming that this is the maximal possible concentration of petrogenic $n$-alkanes in the sediment samples of our FSPS and that this equally underlies both the even and odd leaf wax compounds from fluvial sediments and (paleo)soils, the proportion of petrogenic $n$-alkanes for each sample can be quantified and calculated as follows:

$$\text{petrogenic contribution (\%)} = \frac{0.007\,\mu g\,g^{-1} \cdot \text{sum of chains}}{n\text{-alkane concentration } \mu g\,g^{-1}} \cdot 100. \quad (1)$$

The sum of chains is the number of $n$-alkane chains from $C_{25}$ to $C_{35}$, and the $n$-alkane concentration is the sum of concentrations from $C_{25}$ to $C_{35}$. In cases where not all shorter chains ($< C_{25}$) could completely be removed from the sample by heating, they will be included in the calculation.

The calculated petrogenic contribution (%) that is assumed to be $^{14}C$ dead (i.e., has an $F^{14}C$ value of 0) can then be subtracted from the measured $F^{14}C$ value to derive the petrogenically corrected $F^{14}C$ value ($F^{14}C_{\text{petro corr}}$):

$$F^{14}C_{\text{petro corr}} = F^{14}C_{\text{measured}} + (F^{14}C_{\text{measured}} \cdot \text{petrogenic contribution} \cdot 0.01). \quad (2)$$

The obtained petrogenically corrected $F^{14}C$ values were then calibrated with IntCal13 to yield calendar ages again. We have to note that error propagation of the calibrated petrogenically corrected ages is difficult, and we simply used the measured $^{14}C$ error of the respective sample before petrogenic correction. This might hold some uncertainty, but when corrected the error should basically become smaller and fall within the measured $^{14}C$ error. We also have to note that calibrated petrogenically corrected ages are based on the maximal possible petrogenic contribution in the sediment samples from our FSPS. However, since the proportion of petrogenic $n$-alkanes is not necessarily constant over our FSPS and can become diluted in the sediment samples by sediment material that was not derived from black clay shales and/or the slight loss of long-chain $n$-alkanes during heating (see discussion in Sect. 3.1), the leaf-wax-derived $n$-alkane ages lie in between the heated and petrogenically corrected ages.

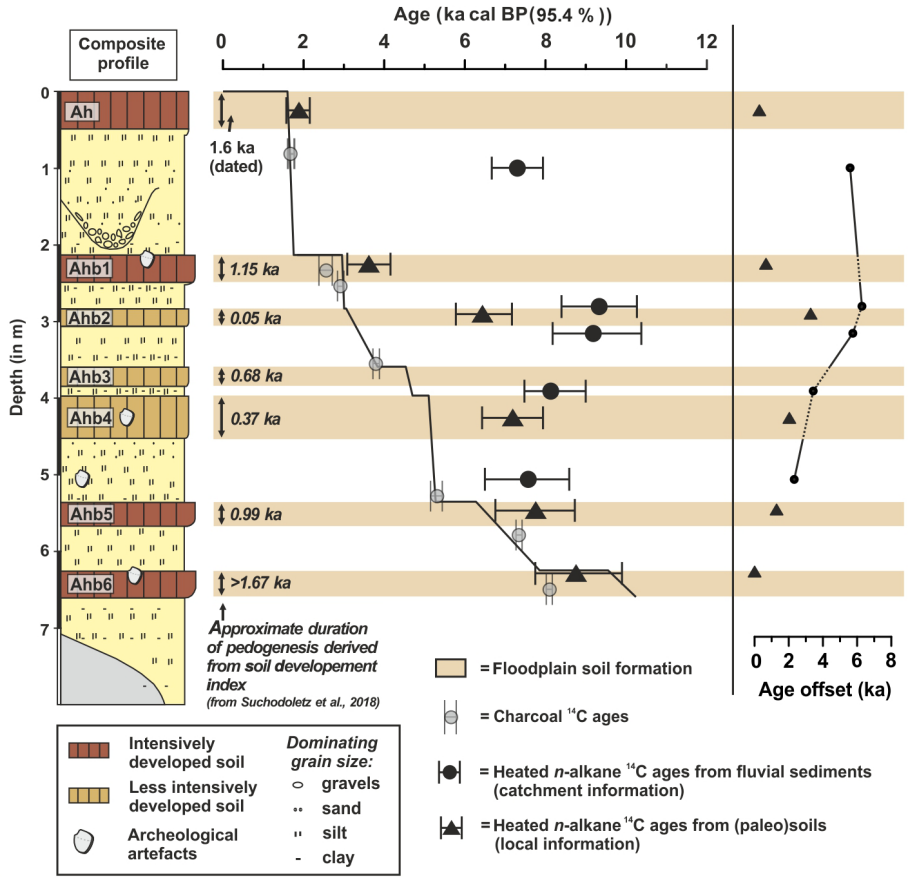


**Figure 6.** Chronostratigraphy of the investigated FSPS with *n*-alkane $^{14}$C ages after heating with 120 °C for 8 h from (paleo)soils and fluvial sediment layers. $^{14}$C ages are given as calibrated age ranges in ka cal BP (95.4 %) with the calibrated median age. Please note the shorter timescale (*x* axis) compared with Fig. 5.

As illustrated in Fig. 7, the maximal possible petrogenic contribution from petrogenic *n*-alkanes can be quantified and corrected for by this approach. Maximal possible petrogenic contributions are relatively high with ∼ 0.8 to 2.0 ka throughout the investigated FSPS. Compared to the fluvial sediments, the (paleo)soils show lower contributions of petrogenic *n*-alkanes. Due to generally higher total *n*-alkane concentrations in the upper part of the FSPS, the relative proportion of the maximal possible petrogenic contribution generally decreases from bottom to top (Fig. 7).

### 3.4 On-site leaf wax *n*-alkane formation versus pre-aging and reworking

Since the petrogenic *n*-alkanes could effectively be removed by heating and correction for maximal petrogenic contributions, the remaining *n*-alkanes should mostly derive from leaf waxes. Accordingly, their age offsets to the sediment layers in the FSPS in which they are buried became smaller. However, the age offsets still reach up to several millennia and vary over the FSPS. These have to be regarded as minimal age offsets since the correction for petrogenic contributions yielded maximal possible values. These offsets generally differ between (paleo)soils and fluvial sediment layers (Fig. 7).

#### 3.4.1 Fluvial sediment layers

Calculated petrogenically corrected minimal age offsets for the leaf wax *n*-alkanes from fluvial sediment layers range between ∼ 0.4 and ∼ 5.0 ka. They are distinctively larger in the upper part of the FSPS, i.e., in the fluvial sediment layers above Ahb1, Ahb2 and Ahb3. In the lower part of the FSPS, below Ahb3 and Ahb4, corrected age offsets strongly decrease and are only slightly off from the timing of sedimentation (Fig. 7). We interpret these variable age offsets to be caused by different degrees of pre-aging and reworking of OC and leaf wax *n*-alkanes, which can mainly be caused by three different effects.

i. *Different degrees of pre-aging and reworking of OC and leaf wax n-alkanes.* The proportion of recent to subrecent versus pre-aged and reworked OC and leaf wax *n*-alkanes in FSPS is primarily controlled by the intensity of physical erosion in the catchment (Hilton et al., 2012; Smith et al., 2013; Galy et al., 2015). Thus,

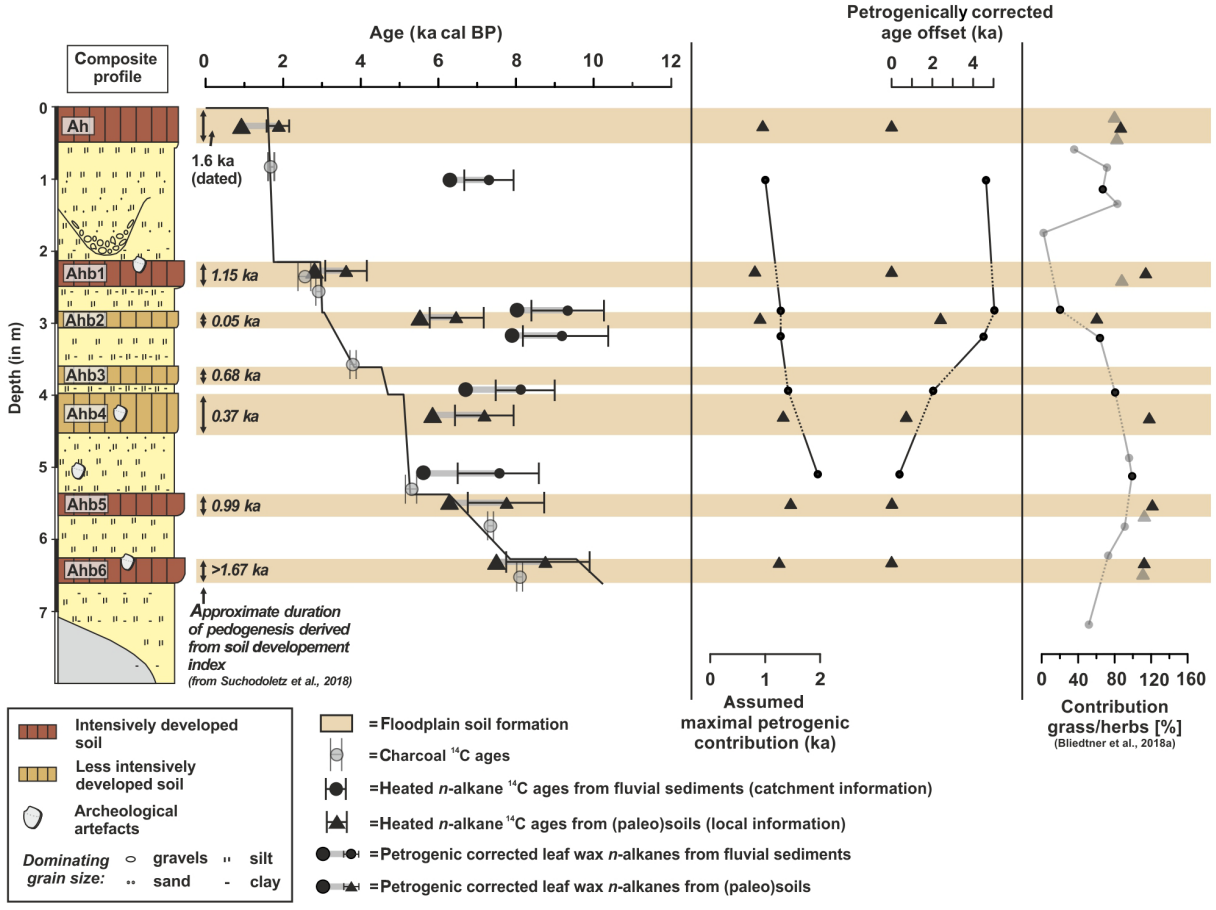


**Figure 7.** Chronostratigraphy of the investigated FSPS with leaf wax *n*-alkane $^{14}$C ages corrected for maximal possible petrogenic contributions from catchment-derived Jurassic black clay shales. Contributions of grasses and herbs have been previously reported by Bliedtner et al. (2018a). Data points showing the percentages of grasses and herbs derived from Bliedtner et al. (2018a) that do not have direct $^{14}$C age information from this study are plotted in a transparent way, and data points with such $^{14}$C age information are shown without transparency.

larger $^{14}$C age offsets in the upper part of our FSPS indicate more intensive and profound erosion in the upper Alazani subcatchment during the last 4 ka cal BP, leading to a relatively large-scale mobilization of pre-aged OC and leaf wax *n*-alkanes compared with recent to subrecent ones. In contrast, smaller age offsets in the lower part of the FSPS indicate less intensive and profound erosion before ca. 4 ka cal BP, when larger relative amounts of recent to subrecent OC and leaf wax *n*-alkanes were mobilized (see Fig. 7).

ii. *Different durations of on-site soil formation and the associated buildup of OC and leaf wax n-alkanes in catchment soils.* Provided they were not occasionally eroded, recent soils continuously built up during the Holocene, and thereby the mean age of soil OC and leaf wax *n*-alkanes became successively older (Smittenberg et al., 2006; Gierga et al., 2016). Therefore, OC and *n*-alkanes that were eroded after a longer time of soil development during the late Holocene should exhibit larger mean age offsets than those that were eroded during the early or middle Holocene, i.e., after a shorter time of soil development. Thus, even in case of a constant proportion of recent to subrecent versus pre-aged and reworked OC and leaf wax *n*-alkanes in the sediments, a systematic increase in the age offsets throughout the Holocene should be expected.

iii. *Sediment (dis)connectivity (Leithold et al., 2006).* Disconnectivity in a hydrological catchment describes blockages like sediment sinks and storages that temporarily interrupt longitudinal, lateral and vertical sediment delivery (Fryirs, 2013), leading to increasing OC and leaf wax *n*-alkane age offsets. However, because of its relatively small size of $\sim 1100\,km^2$ and the steep average slopes of $\sim 20°$ (Fig. 2b), the upper Alazani subcatchment has high sediment connectivity. This is also demonstrated by the general absence of fine-grained overbank sediments upstream of the confluence of the uppermost parts of the Alazani and Ilto rivers. There-

fore, most of the fine-grained material in the investigated FSPS must have been eroded relatively shortly before final deposition, i.e., without a significant time lag between both processes (Bliedtner et al., 2018a; von Suchodoletz et al., 2018). Altogether, since disconnectivity effects in the upper Alazani subcatchment are apparently negligible and although the continuous buildup of OC and leaf wax $n$-alkanes in catchment soils can contribute to the age offsets, strongly increasing age offsets after $\sim 4$ ka cal BP are most likely a result of increased erosion due to intensified regional anthropogenic activity since $\sim 4.5$ ka cal BP (Akhundov, 2004).

#### 3.4.2 (Paleo)soils

For the intensively developed (paleo)soils Ah, Ahb1, Ahb5 and Ahb6, petrogenically corrected leaf wax $n$-alkane ages show no minimal age offsets and thus fall into the periods of soil formation (Fig. 7). In contrast, minimal age offsets of the less intensively developed paleosols Ahb4 and Ahb2 strongly increase up to $\sim 2.4$ ka (Fig. 7). Thus, in these weakly developed paleosols the on-site leaf wax $n$-alkane signal from local biomass decomposition is still much more strongly biased by inherited pre-aged and reworked leaf wax $n$-alkanes from their fluvial parent material compared to the intensively developed (paleo)soils. In the latter, the longer duration of soil development must have had constantly incorporated locally derived leaf wax $n$-alkanes that fully overprinted the previously deposited leaf wax $n$-alkanes from their fluvial parent material.

Taken together, whereas relatively large age offsets between leaf wax $n$-alkane formation and deposition can occur in less intensively developed paleosols and fluvial sediment layers, leaf wax $n$-alkane ages from intensively developed (paleo)soils reflect most reliably the timing of their formation.

### 3.5 Implications for leaf wax $n$-alkane-based paleoenvironmental reconstructions from our FSPS

The vegetation distribution of deciduous trees and shrubs as well as grasses and herbs can be derived from the leaf wax $n$-alkane distribution pattern and was previously described by Bliedtner et al. (2018a) for the investigated FSPS. There, the vegetation distribution is expressed in a two-component mixing equation as the grass / herb ratio based on regional end-members and corrected for possible degradation effects (Fig. 7). We have to mention that absolute grass and herb percentages can exceed 100 %, but those should not be overinterpreted and rather be considered as semiquantitative estimates.

#### 3.5.1 Fluvial sediment layers

The interpretation of catchment-derived leaf wax $n$-alkanes from the fluvial sediment layers is very challenging as they show variable minimal age offsets of $\sim 0.3$ to 4.7 ka over the investigated FSPS. It appears that all dated leaf wax $n$-alkanes from fluvial sediment layers in the FSPS must have formed during a similar period in the middle Holocene, between $\sim 8$ and $\sim 5.6$ ka cal BP (Fig. 8). However, their formation could also have started some centuries earlier since the petrogenic correction only provides a minimal estimate for the age offsets (Fig. 7). Despite the variable-corrected ages, some rough paleovegetational trends can be derived from the fluvial sediment layers of the FSPS. A dominance of deciduous tree- and shrub-derived leaf wax $n$-alkanes in fluvial sediments between ca. 390 and 170 cm indicates that larger parts of the upper Alazani subcatchment must have been forested during the middle Holocene (Fig. 7), and dominating grass- and herb-derived leaf wax $n$-alkanes from the lower (between ca. 575 and 480 cm) and uppermost (above ca. 130 cm) parts of the FSPS with similar ages indicate that other parts of the catchment must have been covered by grass or herb vegetation during the same period (Fig. 8). Therefore, catchment-derived leaf wax $n$-alkanes were not constantly eroded relatively shortly after their formation as was previously suggested by Bliedtner et al. (2018a). Instead, large-scale erosion of leaf wax $n$-alkanes with similar middle Holocene ages must have occurred in different parts of the subcatchment during different periods (Fig. 8).

#### 3.5.2 (Paleo)soils

Our results show that the petrogenically corrected leaf wax $n$-alkane $^{14}$C ages from the intensively developed (paleo)soils Ah, Ahb1, Ahb5 and Ahb6 that were all formed for at least 1 kyr generally agree with the independent $^{14}$C ages derived from charcoal (Fig. 7). That means that the respective leaf wax proxies from such soils, e.g., the commonly used ACL, OEP and stable hydrogen–carbon isotopes, give reliable paleoenvironmental information about the leaf wax $n$-alkane signal formed on-site. Thus, since leaf waxes formed on-site dominate the $n$-alkane signal in the intensively developed (paleo)soils of the FSPS in the upper Alazani valley, they are chronostratigraphically consistent and not affected by pre-aging and reworking effects. These $n$-alkanes indicate higher percentages of grasses and herbs at the studied site throughout the Holocene (Bliedtner et al., 2018a; Figs. 7 and 8). The natural potential vegetation in the upper Alazani lowlands is elm–oak–vine forest rather than grassland (Connor and Kvavadze, 2008), and accordingly coniferous and deciduous trees have been reported by pollen analyses from buried soil profiles for the neighboring Iori lowlands before 5 ka cal BP (Gogichaishvili, 1984; for location see Fig. 1 and record in Fig. 8). Therefore, increased anthropogenic activity is the most likely

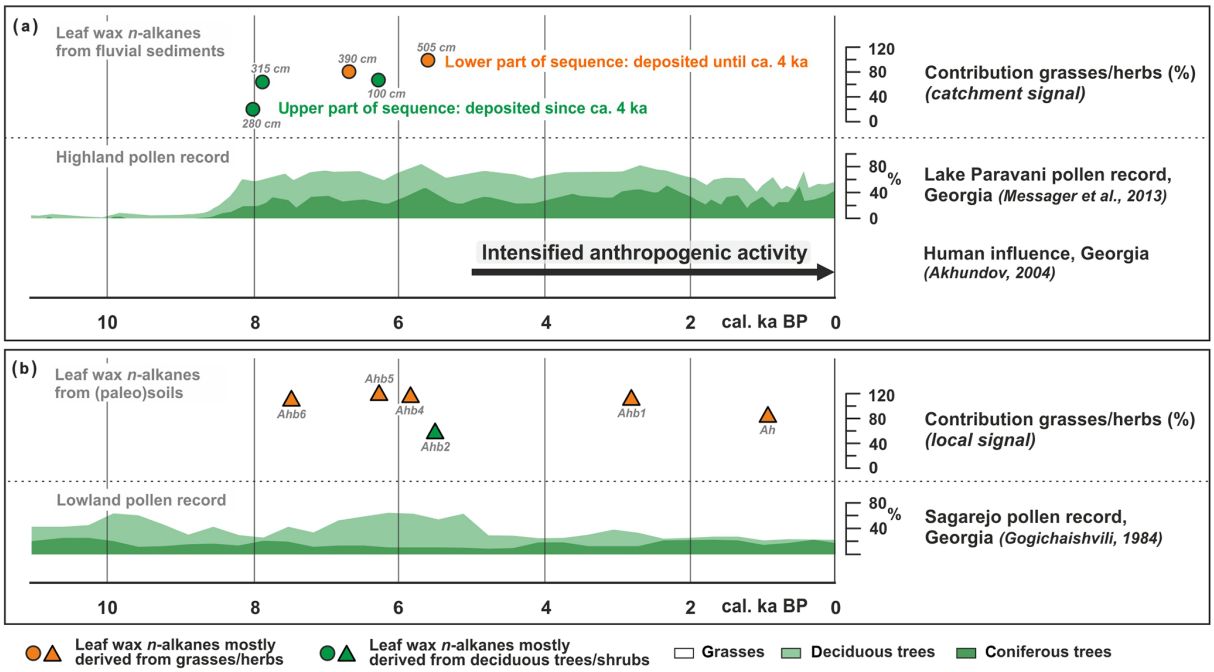


**Figure 8. (a)** Leaf wax *n*-alkane record from fluvial sediments from the investigated FSPS compared with the regional highland pollen record from Lake Paravani in southern Georgia (Messager et al., 2013; for location see Fig. 1) and with generally increasing human activity in the region (Akhundov, 2004). **(b)** Leaf wax *n*-alkane record from (paleo)soils from the investigated FSPS compared with the lowland Sagarejo sediment section (Gogichaishvili, 1984; for locations see Fig. 1). Contributions of grasses and herbs derived from Bliedtner et al. (2018a; see highlighted samples in Fig. 7) are plotted with the corresponding $^{14}$C ages from this study.

cause for the observed grass and herb dominance in the (paleo)soils at the studied site for most of the Holocene (Bliedtner et al., 2018a). Accordingly, anthropogenic influence dating back to ∼ 8 ka cal BP is documented by archeological artifacts in paleosol Ahb6 at the studied site (Fig. 3), and regional anthropogenic activity has generally intensified since ∼ 4.5 ka cal BP (Akhundov, 2004; see Fig. 8). Compared with the intensively developed (paleo)soils, relatively large offsets between the petrogenically corrected leaf wax *n*-alkane $^{14}$C ages and the independent charcoal $^{14}$C ages are found for the less intensively developed paleosols Ahb4 and Ahb2. This should be caused by the larger proportion of preaged and reworked leaf wax *n*-alkanes from their fluvial parent material compared with the signal formed on-site. This is further demonstrated by the significantly smaller minimal age offset of ∼ 0.7 ka for paleosol Ahb4 that had formed for ca. 400 years compared to the minimal age offset of ∼ 2.2 ka for paleosol Ahb2 that had only formed for some decades (Fig. 7). Given that their signal is strongly dominated by inherited *n*-alkanes from fluvial sediment layers, the dominance of deciduous trees and shrubs in the weakly developed paleosol Ahb2 does not affect the general picture of a dominance of grass and herb vegetation at the investigated site throughout the Holocene (Fig. 8).

### 3.5.3 Paleoenvironmental reconstruction

Although our leaf wax *n*-alkane $^{14}$C ages do not support the leaf wax *n*-alkane-based paleovegetation interpretation of the previous study of Bliedtner et al. (2018a) in every detail, they confirm its main findings:

- Despite other results from a neighboring pollen archive in the Iori floodplain near Sagarejo (Gogichaishvili, 1984; for location see Fig. 1 and record in Fig. 8), the upper Alazani floodplain has been dominated by grass and herb vegetation throughout the Holocene. This was most probably caused by anthropogenic activity with increased land use.

- At least parts of the upper Alazani subcatchment were covered with deciduous trees and shrubs during the middle Holocene between ∼ 8 and ∼ 5.6 ka cal BP. No older ages were determined from leaf wax *n*-alkanes derived from this type of vegetation. Therefore, it is very likely that this marks the beginning of postglacial reforestation in the upper Alazani subcatchment, although the start of reforestation could also have occurred some centuries earlier since the petrogenic correction only provides a minimal estimate for the age offsets. This corroborates previous pollen data that suggest a delayed regional postglacial reforestation compared with western and central Europe between ca. 9 to

6 ka cal BP (Lake Urmia: Bottema, 1986; Lake Van: Litt et al., 2009; Lake Paravani: Messager et al., 2013; for locations see Fig. 1 and record from Lake Paravani in Fig. 8).

– Leaf wax $n$-alkanes that were formed during the middle Holocene and were deposited before ca. 4 ka cal BP dominantly originate from grass and herb vegetation. In contrast, most leaf wax $n$-alkanes that were formed during a similar period of the middle Holocene but were deposited after ca. 4 ka cal BP originate from deciduous trees and shrubs. This suggests the start of large-scale erosion around ca. 4 ka cal BP in those parts of the upper Alazani subcatchment that were covered by deciduous forest vegetation, whereas prior to that period mostly grassland soils were eroded. Furthermore, larger age offsets between biomarker formation and deposition after ca. 4 ka cal BP suggest more profound erosion processes with a relatively larger mobilization of pre-aged leaf wax $n$-alkanes since that time. This finding agrees with the observation that settlement at higher altitudes of the Greater Caucasus generally started around 4.5 ka cal BP (Akhundov, 2004; Fig. 8).

## 4 Conclusions

During this study, we dated leaf wax $n$-alkanes from a fluvial sediment–paleosol sequence (FSPS) along the upper Alazani in eastern Georgia by compound-class $^{14}$C dating to investigate their potential for paleoenvironmental reconstructions. Our study gave the following results:

– Preheating of the $n$-alkane fraction with 120 °C for 8 h before compound-class $^{14}$C dating effectively removed the short-chain $n$-alkanes ($< C_{25}$). These included a part of the petrogenic $n$-alkane contribution from Jurassic black clay shales from the upper catchment.

– Remaining petrogenic contributions of the long-chain $n$-alkanes ($\geq C_{25}$) were estimated and corrected for by applying a simple constant petrogenic-correction factor that is based on $n$-alkane concentrations in a Jurassic black clay shale sample from the upper Alazani subcatchment. The corrected $n$-alkane $^{14}$C ages from the FSPS were younger than without correction and are much closer to the leaf-wax-derived $n$-alkane age information.

– A part of the petrogenically corrected leaf wax $n$-alkanes still showed relatively large age offsets between their formation and final deposition into the FSPS, indicating different degrees of pre-aging and reworking. While there is no offset for leaf wax $n$-alkanes from intensively developed (paleo)soils, which indicates a dominance of local leaf wax $n$-alkanes produced on-site, the offsets for leaf wax $n$-alkanes from less intensively developed paleosols are much larger. This can possibly be explained with a larger relative proportion of inherited leaf wax $n$-alkanes from their fluvial parent material. Accordingly, the offsets in fluvial sediment layers are even larger and show values up to several thousand years. Since all dated leaf wax $n$-alkanes from fluvial sediment layers show similar middle Holocene ages between $\sim$ 8 and $\sim$ 5.6 ka cal BP irrespective of their stratigraphic position in the FSPS, the age offsets generally increase towards the top of the sequence. This indicates a greater relative proportion of pre-aged and reworked compared with recent to subrecent leaf wax $n$-alkanes in fluvial sediments deposited after ca. 4 ka cal BP.

– Leaf waxes from intensively developed (paleo)soils showed a dominance of grass and herb vegetation at the studied site throughout the Holocene. This was most likely caused by anthropogenic influence since $\sim$ 8 ka cal BP. Middle Holocene $n$-alkanes from fluvial sediment layers in different parts of the FSPS indicate deciduous trees and shrubs as well as grasses and herbs in the upper Alazani subcatchment since $\sim$ 8 ka cal BP at the latest, indicating a delayed postglacial reforestation of parts of the upper Alazani subcatchment since ca. 9–8 ka cal BP. Compared with western and central Europe, this indicates a delayed start of reforestation of some millennia and is in accordance with other regional pollen studies. Whereas the leaf wax $n$-alkanes that were deposited prior to ca. 4 ka cal BP show a dominance of grasses and herbs, those that were deposited after ca. 4 ka cal BP show a dominant origin from deciduous trees and shrubs. This indicates the start of large-scale erosion in deciduous-forest-covered parts of the subcatchment since that period.

Our results demonstrate that compound-class $^{14}$C dating of $n$-alkanes in FSPSs is an important and valuable tool to investigate their age and origin since varying proportions of both local and catchment-derived leaf wax $n$-alkanes are found in these archives. Therefore, this step is a mandatory precondition not only for robust leaf wax $n$-alkane-based paleoenvironmental reconstructions from FSPSs but also from other kinds of sediment archives with hydrological catchments such as lake and marine sediments. Generally, for leaf wax $n$-alkane-based paleoenvironmental studies in such sediment archives we recommend selecting (i) catchments without carbon-rich sediment rocks containing petrogenic $n$-alkanes and (ii) relatively small catchments with short mean transfer times between leaf wax $n$-alkane formation and deposition.

*Data availability.* The dataset used for this study is provided as a results table in the paper.

*Author contributions.* MB, HvS and RZ designed the study. MB and HvS collected samples. MB, IS, CW, GS and MH carried out the laboratory and analytical analyses. All authors contributed to the writing of the paper and data discussion.

*Competing interests.* The authors declare that they have no conflict of interest.

*Acknowledgements.* We thank Ulrich Göres (Dresden) and Giorgi Merebashvili (Tbilisi) for their help during fieldwork. We thank Ulrich Hanke and two anonymous reviewers for their valuable and helpful comments on this paper.

*Financial support.* This research has been supported by the Swiss National Science Foundation (grant no. P00P2-150590).

*Review statement.* This paper was edited by Laurent Pfister and reviewed by Ulrich Hanke and one anonymous referee.

## References

Adamia, S., Alania, V., Chabukiani, A., Chichua, G., Enukidze, O., and Sadradze, N.: Evolution of the Late Cenozoic basins of Georgia (SW Caucasus): A review, Geol. Soc. Lond. Spec. Publ., 340, 239–259, https://doi.org/10.1144/SP340.11, 2010.

Akhundov, T.: South Caucasus in the Neolithic and early Bronze Age: The question of epochs and periods, in: A view from the highlands: Archaeological studies in honour of Charles Burney, edited by: Sagona, A., Ancient Near Eastern studies Supplement, 12, Peeters, Herent, 421–436, 2004.

Blair, N. E. and Aller, R. C.: The fate of terrestrial organic carbon in the marine environment, Annu. Rev. Mar. Sci., 4, 401–423, https://doi.org/10.1146/annurev-marine-120709-142717, 2012.

Bliedtner, M., Zech, R., Kühn, P., Schneider, B., Zielhofer, C., and von Suchodoletz, H.: The potential of leaf wax biomarkers from fluvial soil-sediment sequences for paleovegetation reconstructions – Upper Alazani River, central southern Greater Caucasus (Georgia), Quaternary Sci. Rev., 196, 62–79, https://doi.org/10.1016/j.quascirev.2018.07.029, 2018a.

Bliedtner, M., Schäfer, I. K., Zech, R., and von Suchodoletz, H.: Leaf wax n-alkanes in modern plants and topsoils from eastern Georgia (Caucasus) – implications for reconstructing regional paleovegetation, Biogeosciences, 15, 3927–3936, https://doi.org/10.5194/bg-15-3927-2018, 2018b.

Bottema, S.: A late quaternary pollen diagram from Lake Urmia (Northwestern Iran), Rev. Palaeobot. Palynol., 47, 241–261, https://doi.org/10.1016/0034-6667(86)90039-4, 1986.

Connor, S. E. and Kvavadze, E. V.: Modelling late Quaternary changes in plant distribution, vegetation and climate using pollen data from Georgia, Caucasus, J. Biogeogr., 36, 529–545, https://doi.org/10.1111/j.1365-2699.2008.02019.x, 2008.

Connor, S. E., Thomas, I., Kvavadze, E. V., Arabuli, G. J., Avakov, G. S., and Sagona, A.: A survey of modern pollen and vegetation along an altitudinal transect in southern Georgia, Caucasus region, Rev. Palaeobot. Palynol., 129, 229–250, https://doi.org/10.1016/j.revpalbo.2004.02.003, 2004.

Douglas, P. M.J., Pagani, M., Eglinton, T. I., Brenner, M., Hodell, D. A., Curtis, J. H., Ma, K. F., and Breckenridge, A.: Pre-aged plant waxes in tropical lake sediments and their influence on the chronology of molecular paleoclimate proxy records, Geochim. Cosmochim. Ac., 141, 346–364, https://doi.org/10.1016/j.gca.2014.06.030, 2014.

Douglas, P. M. J., Pagani, M., Eglinton, T. I., Brenner, M., Curtis, J. H., Breckenridge, A., and Johnston, K.: A long-term decrease in the persistence of soil carbon caused by ancient Maya land use, Nat. Geosci., 5, 645–649, https://doi.org/10.1038/s41561-018-0192-7, 2018.

Eglinton, T. I. and Eglinton, G.: Molecular proxies for paleoclimatology, Earth Planet. Sc. Lett., 275, 1–16, https://doi.org/10.1016/j.epsl.2008.07.012, 2008.

Feng, X., Vonk, J. E., van Dongen, B. E., Gustafsson, Ö., Semiletov, I. P., Dudarev, O. V., Wang, Z., Montluçon, D. B., Wacker, L., and Eglinton, T. I.: Differential mobilization of terrestrial carbon pools in Eurasian Arctic river basins, P. Natl. Acad. Sci. USA, 110, 14168–14173, https://doi.org/10.1073/pnas.1307031110, 2013.

Ficken, K. J., Li, B., Swain, D. L., and Eglinton, G.: An $n$-alkane proxy for the sedimentary input of submerged/floating freshwater aquatic macrophytes, Org. Geochem., 31, 745–749, https://doi.org/10.1016/S0146-6380(00)00081-4, 2000.

Forte, A. M., Cowgill, E., Bernardin, T., Kreylos, O., and Hamann, B.: Late Cenozoic deformation of the Kura fold-thrust belt, southern Greater Caucasus, Geol. Soc. Am. Bull., 122, 465–486, https://doi.org/10.1130/B26464.1, 2010.

Fryirs, K.: (Dis)Connectivity in catchment sediment cascades: A fresh look at the sediment delivery problem, Earth Surf. Proc. Land., 38, 30–46, https://doi.org/10.1002/esp.3242, 2013.

Galy, V. and Eglinton, T.: Protracted storage of biospheric carbon in the Ganges–Brahmaputra basin, Nat. Geosci., 4, 843–847, https://doi.org/10.1038/ngeo1293, 2011.

Galy, V., Beyssac, O., France-Lanord, C., and Eglinton, T.: Recycling of graphite during Himalayan erosion: a geological stabilization of carbon in the crust, Science, 322, 943–945, https://doi.org/10.1126/science.1161408, 2008.

Galy, V., Peucker-Ehrenbrink, B., and Eglinton, T.: Global carbon export from the terrestrial biosphere controlled by erosion, Nature, 521, 204–207, https://doi.org/10.1038/nature14400, 2015.

Gamkrelidze, I. P.: Geological map of Georgia 1 : 500, 000, Georgian State Department of Geology and National Oil Company "SAQNAFTOBI", 2003.

Gierga, M., Hajdas, I., van Raden, U. J., Gilli, A., Wacker, L., Sturm, M., Bernasconi, S. M., and Smittenberg, R. H.: Long-stored soil carbon released by prehistoric land use: Evidence from compound-specific radiocarbon analysis on Soppensee lake sediments, Quaternary Sci. Rev., 144, 123–131, https://doi.org/10.1016/j.quascirev.2016.05.011, 2016.

Gogichaishvili, L. K.: Vegetational and climatic history of the western part of the Kura River Basin, in: Palaeoclimates, Palaeoenvironments and Human Communities in the Eastern Mediterranean Region in Later Prehistory, edited by: Bintliff, J. L. and van Zeist, W., BAR International Series, 133, 325–341, 1984.

Haas, M., Bliedtner, M., Borodynkin, I., Salazar, G., Szidat, S., Eglinton, T. I., and Zech, R.: Radiocarbon Dating of Leaf Waxes in the Loess-Paleosol Sequence Kurtak, Central Siberia, Radiocarbon, 59, 165–176, https://doi.org/10.1017/RDC.2017.1, 2017.

Häggi, C., Eglinton, T. I., Zech, W., Sosin, P., and Zech, R.: A 250 ka leaf-wax $\delta$D record from a loess section in Darai Kalon, Southern Tajikistan, Quaternary Sci. Rev., 208, 118–128, https://doi.org/10.1016/j.quascirev.2019.01.019, 2019.

Hedges, J. I., Clark, W. A., Quay, P. D., Richey, J. E., Devol, A. H., and Santos, U. D. M.: Compositions and fluxes of particulate organic material in the Amazon River, Limnol. Oceangr., 31, 717–738, https://doi.org/10.4319/lo.1986.31.4.0717, 1986.

Hilton, R. G., Galy, A., Hovius, N., Horng, M.-J., and Chen, H.: Efficient transport of fossil organic carbon to the ocean by steep mountain rivers: An orogenic carbon sequestration mechanism, Geology, 39, 71–74, https://doi.org/10.1130/G31352.1, 2010.

Hilton, R. G., Galy, A., Hovius, N., Kao, S.-J., Horng, M.-J., and Chen, H.: Climatic and geomorphic controls on the erosion of terrestrial biomass from subtropical mountain forest, Global Biogeochem. Cy., 26, GB3014, https://doi.org/10.1029/2012GB004314, 2012.

Leithold, E. L., Blair, N. E., and Perkey, D. W.: Geomorphologic controls on the age of particulate organic carbon from small mountainous and upland rivers, Global Biogeochem. Cy., 20, GB3022, https://doi.org/10.1029/2005GB002677, 2006.

Li, G., Li, L., Tarozo, R., Longo, W. M., Wang, K. J., Dong, H., and Huang, Y.: Microbial production of long-chain $n$-alkanes: Implication for interpreting sedimentary leaf wax signals, Org. Geochem., 115, 24–31, https://doi.org/10.1016/j.orggeochem.2017.10.005, 2018.

Litt, T., Krastel, S., Sturm, M., Kipfer, R., Örcen, S., Heumann, G., Franz, S. O., Ülgen, U. B., and Niessen, F.: 'PALEOVAN', International Continental Scientific Drilling Program (ICDP): Site survey results and perspectives, Quaternary Sci. Rev., 28, 1555–1567, https://doi.org/10.1016/j.quascirev.2009.03.002, 2009.

Lydolph, P. E. (Ed.): Climates of the Soviet Union: [138 Tab.], World survey of climatology, 7, Elsevier, Amsterdam, 443 pp., 1977.

Makou, M., Eglinton, T., McIntyre, C., Montluçon, D., Antheaume, I., and Grossi, V.: Plant Wax $n$-Alkane and $n$-Alkanoic Acid Signatures Overprinted by Microbial Contributions and Old Carbon in Meromictic Lake Sediments, Geophys. Res. Lett., 45, 1049–1057, https://doi.org/10.1002/2017GL076211, 2018.

Marwick, T. R., Tamooh, F., Teodoru, C. R., Borges, A. V., Darchambeau, F., and Bouillon, S.: The age of river-transported carbon: A global perspective, Global Biogeochem. Cy., 29, 122–137, https://doi.org/10.1002/2014GB004911, 2015.

Messager, E., Belmecheri, S., Grafenstein, U. von, Nomade, S., Ollivier, V., Voinchet, P., Puaud, S., Courtin-Nomade, A., Guillou, H., Mgeladze, A., Dumoulin, J.-P., Mazuy, A., and Lordkipanidze, D.: Late Quaternary record of the vegetation and catchment-related changes from Lake Paravani (Javakheti, South Caucasus), Quaternary Sci. Rev., 77, 125–140, https://doi.org/10.1016/j.quascirev.2013.07.011, 2013.

Millard, A. R.: Conventions for Reporting Radiocarbon Determinations, Radiocarbon, 56, 555–559, https://doi.org/10.2458/56.17455, 2014.

Ramsey, C.: Bayesian Analysis of Radiocarbon Dates, Radiocarbon, 51, 337–360, https://doi.org/10.1017/S0033822200033865, 2009.

Reimer, P. J., Bard, E., Bayliss, A., Beck, J. W., Blackwell, P. G., Ramsey, C. B., Buck, C. E., Cheng, H., Edwards, R. L., Friedrich, M., Grootes, P. M., Guilderson, T. P., Haflidason, H., Hajdas, I., Hatté, C., Heaton, T. J., Hoffmann, D. L., Hogg, A. G., Hughen, K. A., Kaiser, K. F., Kromer, B., Manning, S. W., Niu, M., Reimer, R. W., Richards, D. A., Scott, E. M., Southon, J. R., Staff, R. A., Turney, C. S. M., and van der Plicht, J.: IntCal13 and Marine13 Radiocarbon Age Calibration Curves 0–50,000 Years cal BP, Radiocarbon, 55, 1869–1887, https://doi.org/10.2458/azu_js_rc.55.16947, 2013.

Ruff, M., Fahrni, S., Gaggeler, H. W., Hajdas, I., Suter, M., Synal, H.-A., Szidat, S., and Wacker, L.: On-line Radiocarbon Measurements of Small Samples Using Elemental Analyzer and MICADAS Gas Ion Source, available at: https://journals.uair.arizona.edu/index.php/radiocarbon/article/view/3429 (last access: 27 April 2020), 2011.

Sachse, D., Radke, J., and Gleixner, G.: $\delta$D values of individual $n$-alkanes from terrestrial plants along a climatic gradient – Implications for the sedimentary biomarker record, Org. Geochem., 37, 469–483, https://doi.org/10.1016/j.orggeochem.2005.12.003, 2006.

Sagheb-Talebi, K., Sajedi, T., and Pourhashemi, M.: Forests of Iran: A treasure from the past, a hope for the future, in: Plant Vegetation, Springer Netherlands, s.l., Dordrecht, 55 pp., 2014.

Salazar, G., Zhang, Y. L., Agrios, K., and Szidat, S.: Development of a method for fast and automatic radiocarbon measurement of aerosol samples by online coupling of an elemental analyzer with a MICADAS AMS, Nucl. Instrum. Meth. Phys. Res. Sect. B, 361, 163–167, https://doi.org/10.1016/j.nimb.2015.03.051, 2015.

Sauer, P. E., Eglinton, T. I., Hayes, J. M., Schimmelmann, A., and Sessions, A. L.: Compound-specific D / H ratios of lipid biomarkers from sediments as a proxy for environmental and climatic conditions, Geochim. Cosmochim. Ac., 65, 213–222, https://doi.org/10.1016/S0016-7037(00)00520-2, 2001.

Schäfer, I. K., Bliedtner, M., Wolf, D., Kolb, T., Zech, J., Faust, D., and Zech, R.: A $\delta^{13}$C and $\delta^{2}$H leaf wax record from the Late Quaternary loess-paleosoil sequence El Paraíso, Central Spain, Palaeogeogr. Palaeocl., 507, 52–59, https://doi.org/10.1016/j.palaeo.2018.06.039, 2018.

Schefuß, E., Schouten, S., and Schneider, R. R.: Climatic controls on central African hydrology during the past 20,000 years, Nature, 437, 1003–1006, https://doi.org/10.1038/nature03945, 2005.

Schefuß, E., Eglinton, T. I., Spencer-Jones, C. L., Rullkötter, J., de Pol-Holz, R., Talbot, H. M., Grootes, P. M., and Schneider, R. R.: Hydrologic control of carbon cycling and aged carbon discharge in the Congo River basin, Nat. Geosci., 9, 687–690, https://doi.org/10.1038/ngeo2778, 2016.

Schwark, L., Zink, K., and Lechterbeck, J.: Reconstruction of postglacial to early Holocene vegetation history in terrestrial Central Europe via cuticular lipid biomarkers and pollen records from lake sediments, Geology, 30, 463, https://doi.org/10.1130/0091-7613(2002)030<0463:ROPTEH>2.0.CO;2, 2002.

Smith, J. C., Galy, A., Hovius, N., Tye, A. M., Turowski, J. M., and Schleppi, P.: Runoff-driven export of particulate organic carbon

from soil in temperate forested uplands, Earth Planet. Sc. Lett., 365, 198–208, https://doi.org/10.1016/j.epsl.2013.01.027, 2013.

Smittenberg, R. H., Eglinton, T. I., Schouten, S., and Damsté, J. S. S.: Ongoing buildup of refractory organic carbon in boreal soils during the Holocene, Science, 314, 1283–1286, https://doi.org/10.1126/science.1129376, 2006.

Szidat, S.: $^{14}$C Analysis and Sample Preparation at the New Bern Laboratory for the Analysis of Radiocarbon with AMS (LARA), Radiocarbon, 56, 561–566, https://doi.org/10.2458/56.17457, 2014.

Tao, S., Eglinton, T. I., Montluçon, D. B., McIntyre, C., and Zhao, M.: Pre-aged soil organic carbon as a major component of the Yellow River suspended load: Regional significance and global relevance, Earth Planet. Sc. Lett., 414, 77–86, https://doi.org/10.1016/j.epsl.2015.01.004, 2015.

von Suchodoletz, H., Zielhofer, C., Hoth, S., Umlauft, J., Schneider, B., Zeeden, C., Sukhishvili, L., and Faust, D.: North Atlantic influence on Holocene flooding in the southern Greater Caucasus, Holocene, 28, 609–620, https://doi.org/10.1177/0959683617735584, 2018.

Wacker, L., Bonani, G., Friedrich, M., Hajdas, I., Kromer, B., Němec, M., Ruff, M., Suter, M., Synal, H.-A., and Vockenhuber, C.: MICADAS: Routine and High-Precision Radiocarbon Dating, Radiocarbon, 52, 252–262, https://doi.org/10.1017/S0033822200045288, 2010.

Welte, C., Hendriks, L., Wacker, L., Haghipour, N., Eglinton, T. I., Günther, D., and Synal, H.-A.: Towards the limits: Analysis of microscale $^{14}$C samples using EA-AMS, Nucl. Instrum. Meth. Phys. Res. Sect. B, 437, 66–74, https://doi.org/10.1016/j.nimb.2018.09.046, 2018.

Wirth, S. B. and Sessions, A. L.: Plant-wax D / H ratios in the southern European Alps record multiple aspects of climate variability, Quaternary Sci. Rev., 148, 176–191, https://doi.org/10.1016/j.quascirev.2016.07.020, 2016.

Zech, M., Kreutzer, S., Zech, R., Goslar, T., Meszner, S., McIntyre, C., Häggi, C., Eglinton, T., Faust, D., and Fuchs, M.: Comparative $^{14}$C and OSL dating of loess-paleosol sequences to evaluate post-depositional contamination of *n*-alkane biomarkers, Quatern. Res., 87, 180–189, https://doi.org/10.1017/qua.2016.7, 2017.